Nuclear Instruments and Methods in Physics Research A 845 (2017) 69–71

Contents lists available at ScienceDirect

Nuclear Instruments and Methods in Physics Research A

journal homepage: www.elsevier.com/locate/nima

High-resolution three-dimensional imaging of a depleted CMOS sensor using an edge Transient Current Technique based on the Two Photon Absorption process (TPA-eTCT)

Marcos Fernández García [a,*], Javier González Sánchez [a], Richard Jaramillo Echeverría [a], Michael Moll [b], Raúl Montero Santos [c], David Moya [a], Rogelio Palomo Pinto [d], Iván Vila [a]

[a] Instituto de Física de Cantabria (CSIC-UC), Avda. los Castros s/n, E-39005 Santander, Spain
[b] CERN, Organisation europénne pour la recherche nucléaire, CH-1211 Genéve 23, Switzerland
[c] SGIker Laser Facility, UPV/EHU, Sarriena, s/n - 48940 Leioa-Bizkaia, Spain
[d] Departamento de Ingeniería Electrónica, Escuela Superior de Ingenieros Universidad de Sevilla, Spain

ARTICLE INFO

Article history:
Received 24 March 2016
Received in revised form
10 May 2016
Accepted 17 May 2016
Available online 19 May 2016

Keywords:
Particle tracking pixel detectors
Two Photon Absorption
Transient Current Technique
High-voltage CMOS technology

ABSTRACT

For the first time, the deep n-well (DNW) depletion space of a High Voltage CMOS sensor has been characterized using a Transient Current Technique based on the simultaneous absorption of two photons. This novel approach has allowed to resolve the DNW implant boundaries and therefore to accurately determine the real depleted volume and the effective doping concentration of the substrate. The unprecedented spatial resolution of this new method comes from the fact that measurable free carrier generation in two photon mode only occurs in a micrometric scale voxel around the focus of the beam. Real three-dimensional spatial resolution is achieved by scanning the beam focus within the sample.

1. Introduction

We present the determination of the geometry of the space charge region of a depleted pixel cell using a novel Transient Current Technique (TCT) based on the Two Photon Absorption (TPA [1,2]) physical phenomena. TPA–TCT allows three dimensional mapping sensitivity even for detectors with a shallow depletion depth like CMOS pixel sensors.

In conventional laser TCT [3], silicon detectors are characterized by carrier generation using picosecond laser pulses. The laser wavelength for TCT is above the Si bandgap ($\lambda \leq 1150$ nm) so Single Photon Absorption (SPA) [4], is dominant, inducing carrier generation along the beam path. The laser wavelength also determines spot size and beam divergence. Visible wavelengths (red, green) can be focused to small spots (≤ 1 μm) but penetrate only few micrometers inside Si. Thus, good point spatial resolution is only possible at the surface. Very near infrared wavelengths (typically 1064 nm) can be collimated to ~ 5 μm over several mm depth but carriers are generated along the whole beam path lacking point spatial resolution.

In TPA–TCT, laser wavelength is below the Si bandgap ($\lambda \geq$ 1150 nm), for example 1200–1500 nm. In this regime, only non-linear absorption is relevant [5]. The laser has to generate femtosecond pulses because TPA absorption probability is significant only for very short pulses [6].

The advantage of TPA–TCT is to have both spatial resolution (carrier generation just concentrated around the focal point) and large penetration depth (because out-of-focus intensity does not lead to significant absorption). The approximately ellipsoidal [7] carrier generation volume can be moved inside the sample in all three dimensions, adjusting the focus and displacing the sample. Looking at the detector response, we can establish a strong correlation between transient current and spatial focal point coordinates, being able to resolve detector internal structures and the depletion volume geometry.

Sensors built in High Voltage CMOS process, broadly referred to as HVCMOS sensors [8], are monolithic particle detectors implemented in low resistivity CMOS technology, able to withstand voltages up to 100 V. The deep n-well (DNW) is both the substrate for shallow transistors and the collecting diode. Due to the low resistivity and maximum voltage granted by the technology, the maximum depletion depth is of the order of 10 μm. The version tested here corresponds to the Capacitively Coupled Pixel Detector (CCPD v3) [8].

2. Experimental arrangement

The TPA–TCT experiment was carried out at the SGIker Singular Laser Facility [9]. Femtosecond laser pulses are generated by a

* Corresponding author.

http://dx.doi.org/10.1016/j.nima.2016.05.070

commercial Ti:Sapphire oscillator-regenerative amplifier system (Coherent Mantis-Legend, 1 kHz, 4.0 mJ, 30 fs pulses at 800 nm). A fraction of the amplifier output is used to pump an optical parametric amplifier producing tunable wavelength. The experiments were done at a wavelength of 1300 nm, bandwidth of 12 nm and a pulse duration of 243 fs. A variable neutral density filter regulated the pulse energy at the detector in the range of 10 pJ–1 nJ. Laser intensity was monitored and recorded with a Ge photodiode (Thorlabs, Det50B). IR pulses were focused onto the detector, which is mounted in a high precision three-axis translation stage (Thorlabs, PT3-Z8), with a $\times 100$ objective (Mitutoyo, M Plan Apo SL) giving rise to a beam waist of 1 μm in linear regime. The TPA carrier generation volume was measured by knife edge and *Z*-scan techniques in a standard diode (CNM n-on-p), obtaining values of 0.8 and 13 μm (FWHM) respectively for the radius and length [2].

A transversal cross section of the HVCMOS pixel cell characterized here is shown in Fig. 1 (left). This unirradiated HVCMOS was glued on a PCB designed for transient current measurements, and mounted for edge illumination (laser impinges perpendicularly to the *XY*-plane, see Fig. 1 left). The structure measured was a deep n-well without any embedded NMOS or PMOS transistors, intended for optical test measurements, placed in one corner of the silicon dice (buried in *X*- and *Z*-coordinates, according to mask files). The current picked from the DNW was amplified (Cividec C2-TCT) and recorded using a 2.5 GHz digital oscilloscope. The whole equipment, except the lasers and filters, was isolated in a custom-made Faraday cage, vented with dry air reducing the humidity below 4%. Bias voltage was supplied via front-side implants (P-wells surrounding every DNW), as suggested by the process design rules. In addition to the diode contact to GND, analog and digital grounds of the chip were shorted to a common GND, so that the leakage current from all other deep N-wells of the chip could bypass the diode. The detector was glued to the PCB using conductive glue.

3. Experimental results

A three dimensional scan was realized in two steps. First, the boundaries of the sensitive volume were located in the plane *XY*. Then the laser was focused in *Z*-coordinate, finding the position where the collected signal was at the maximum. Fig. 1 (center) shows a collection charge map (10 ns integration time) as a function of the position of the laser. The location of the implant cannot be inferred from the total charge collection map, thus an accurate determination of the depletion depth is not possible. The size of the charge collecting volume, quoted as Full Width at Half Maximum (FWHM), is 120 $\times$25 μm^2 in *X* and *Y* dimensions, that is, a depletion width of 25 μm, clearly above the expected value.

Fig. 1 (right) shows an *XY* map of the collection time (time lapse between the beginning and end of the signal, where the end of the signal is calculated as the time needed to accumulate 98% of the total charge). A rectangular structure with calculated FWHM~95 $\times$7 μm^2 (location $X \in [0.02, 0.12]$ mm, $Y \sim 0.012$ mm in the collection time map) is identified as the DNW. The implant is surrounded by a region of very short collection times, identified as the drift region ($Y \in [0.016, 0.026]$ mm), followed by a narrow transition towards longer collection times (diffusion region). The maximum collection time in this plot has been fixed to 20 ns. The diode seems to be buried along the *Y*-coordinate since a region of short collection time and non-zero collected charge extends below the implant bottom border ($Y < 0.01$ mm). The actual thickness of this region is, at this moment, not known precisely. Some effects might contribute to an apparent charge collection in this region: reflections of the laser on metal layers on top of the DNW can couple light back to the active area. Photoelectric effect in the same metal might act as a current injection source. Further analysis is required to quantify the importance of these contributions.

Transient currents at each of these regions are compared in Fig. 2. At the drift region, the signal amplitude is high and the collection time short, as corresponds to a depleted volume with high electric field. At the implant, amplitude is smaller but the signal is collected within 10 ns. There, a double peak is observed which hints to a different current peaking time for electrons and holes. Finally, the absence of electric field in the diffusion region makes charge collection very slow. Recombination in this region reduces the total collected charge.

Once the position of the implant is found, depletion can be calculated taking the implant upper border (*Y*~0.016 in Fig. 1 right) as a reference. Fig. 3 overlaps (in arbitrary units), the collection time and collected charge (in 25 ns) profiles along the center of the detector ($X \sim 0.06$ mm in Fig. 1). The position of the implant ($Y \sim 0.012$ mm) is clearly seen in the time profile. After 25 ns, both the implant and bulk collect all the charge. The distance, measured from the rightmost edge of the implant, over which the collection time is minimum, is considered as the depletion thickness. This is shown in Fig. 4, as a function of voltage. For comparison, the FWHM of the charge profile ($X \sim 0.06$ mm) is also displayed. A clear difference between the two depletion depth estimators is observed. By fitting the measured depletion to $w(V)(\mu m) = 0.3\sqrt{\rho(\Omega\ \mathrm{cm})V}$ [10], the resistivity ρ of the bulk can be calculated. The value found, $\rho \sim 15\Omega$ cm, should be compared to the nominal 10 Ω cm.

To complete the three dimensional scan, the beam was pointed at the center of the implant ($(X, Y) = (0.06, 0.012)$ mm in Fig. 1 (right)) and a vertical *Z*-scan was performed. Due to the absence of linear absorption, the laser can be focused on buried structures well inside the silicon dice, as it is the tested implant along the *Z*-direction. The charge integrated in 8 ns along the *Z*-direction is shown in Fig. 5. Due to the wider size of the beam along the propagation direction the reconstructed implant size is the convolution of the implant with the beam. The calculated value is

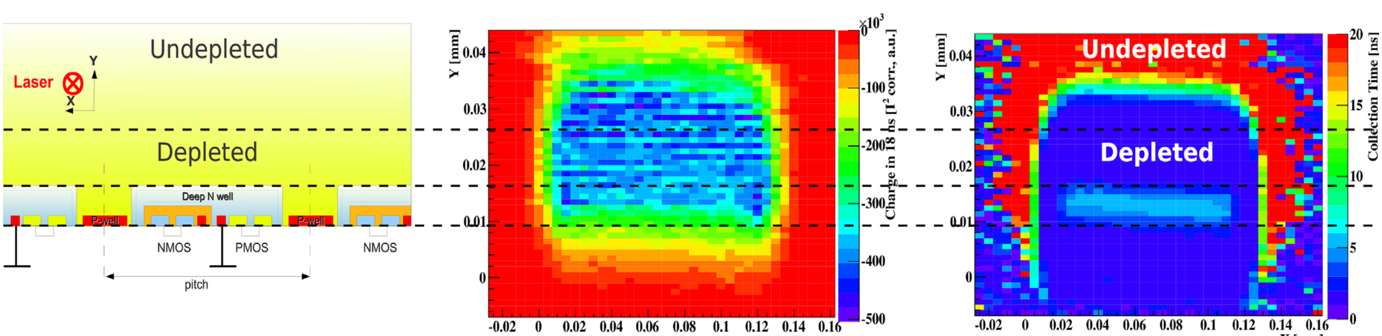

Fig. 1. Left: HVCMOS sketch. Center: charge collection map in 10 ns. Right: Collection time map. Measurements at 20C, −80 V.

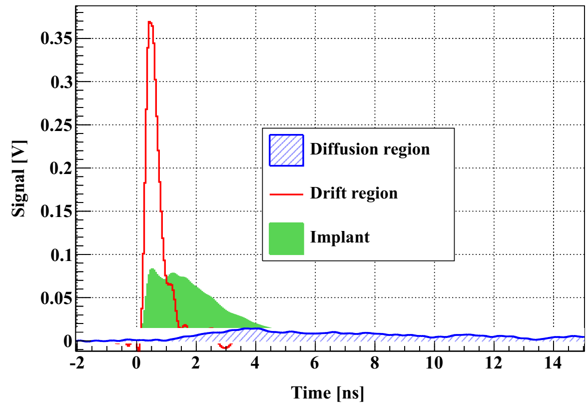

Fig. 2. Transient currents inside the DNW implant, depleted and diffusion regions of an HVCMOS sensor.

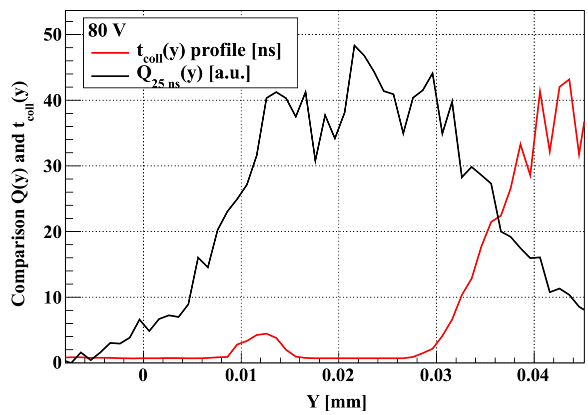

Fig. 3. Comparison (arbitrary vertical units) of collected charge profile (in 25 ns) with the collection time profile.

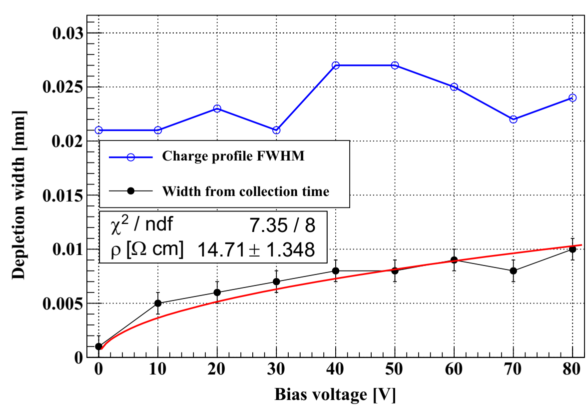

Fig. 4. Comparison of depletion depth calculated using charge profiles only (as in Fig. 1 center) or collection time profiles only (Fig. 1 right).

therefore an overestimation of the actual beam depth along Z. Taking into account that, due to the refraction index of Si, a shift in air of ΔZ_{air} corresponds to $\Delta Z_{Si} = n_{Si}(\lambda)\Delta Z_{\mathrm{air}}$ in Si, the reconstructed depth of the implant is ~106 μm.

4. Conclusions

For the first time, the dimension and geometry of the space charge region of a depleted CMOS pixel cell was accurately measured. This has been possible by measuring the collection time of the carriers, enabling the location of the boundaries of the DNW implant and the determination of the transition between drift and diffusion volumes. From the geometry of the space charge region we can compute the effective doping concentration of the silicon substrate, one of the main design parameters of the HVCMOS technology under optimization.

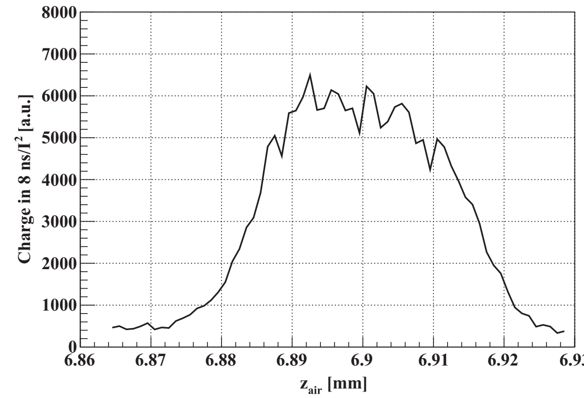

Fig. 5. Collected charge (in 8 ns, room temperature, −80 V) when the beam focus is moved vertically with respect to the detector.

The enabling technology for this achievement is a novel transient current technique based on Two Photon Absorption (TPA–TCT), allowing a submicron spatial resolution in an edge-TCT configuration. TPA–TCT is the only transient current technique able to spatially resolve implants and to discriminate between drift and diffusion. This is because in TPA, focused light generates photocarriers only in a localized volume around the focus. The cross section of this volume is below 1 μm. However, in SPA-TCT, carriers are generated uniformly along the beam, therefore strong focusing only leads to a wide divergence out of the focus, and thus worse spatial resolution.

The results presented here prove the suitability of TPA–TCT as a high-resolution three dimensional probing tool for sensor characterization.

Acknowledgments

This work was performed in the framework of the CERN-RD50 collaboration under the project RD50-2015-03. The project has received funding from the European Commission under the FP7 Research Infrastructures project AIDA, grant agreement no. 262025. This project has been partially supported by the Spanish Ministry of Economy and Competitiveness (MINECO) under grant number FPA2013-48387-C6-1-P. We thank Daniel Muenstermann for providing HVCMOS samples for these measurements.

References

[1] F.R.Palomo. et al., Two photon absorption and carrier generation in semiconductors, 25th RD50 General Meeting.
[2] I. Vila. et al., TPA-TCT: a novel transient current technique based on the two photon absorption process, 25th RD50 General Meeting.
[3] V. Eremin, et al., Nucl. Instrum. Methods Phys. Res. A 372 (3) (1996) 388–398, http://dx.doi.org/10.1016/0168-9002(95)01295-8.
[4] S. Buchner, Army Research Laboratory Doc.ARL-CR 185 (1995) 1–56.
[5] E.W. Van Stryland, et al., Opt. Eng. 24 (4) (1985) 613–623, http://dx.doi.org/10.1117/12.7973538.
[6] A. et al., Q. Rev. Biophys. 2 (38) (2005) 97–166. http://dx.doi.org/10.1017/S0033583505004129.
[7] D. McMorrow, et al., IEEE Trans. Nucl. Sci. NS-49 (6) (2002) 3002–3008, http://dx.doi.org/10.1109/TNS.2002.805337.
[8] I. Peric, J. Instrum. 7 (08) (2012) C08002, http://dx.doi.org/10.1088/1748-0221/7/08/c08002, C08002.
[9] URL ⟨http://www.ehu.eus/en/web/sgiker/laser-tresna-aurkezpena⟩.
[10] H. Spieler, Semiconductor Detector Systems, OUP, Oxford, 2005.